The DNA-Binding Domain Mediates both Nuclear and Cytosolic Functions of p53.

Ariele Viacava Follis, Fabien Llambi, Li Ou, Katherine Baran, Douglas R. Green and Richard W. Kriwacki

Supplementary Information

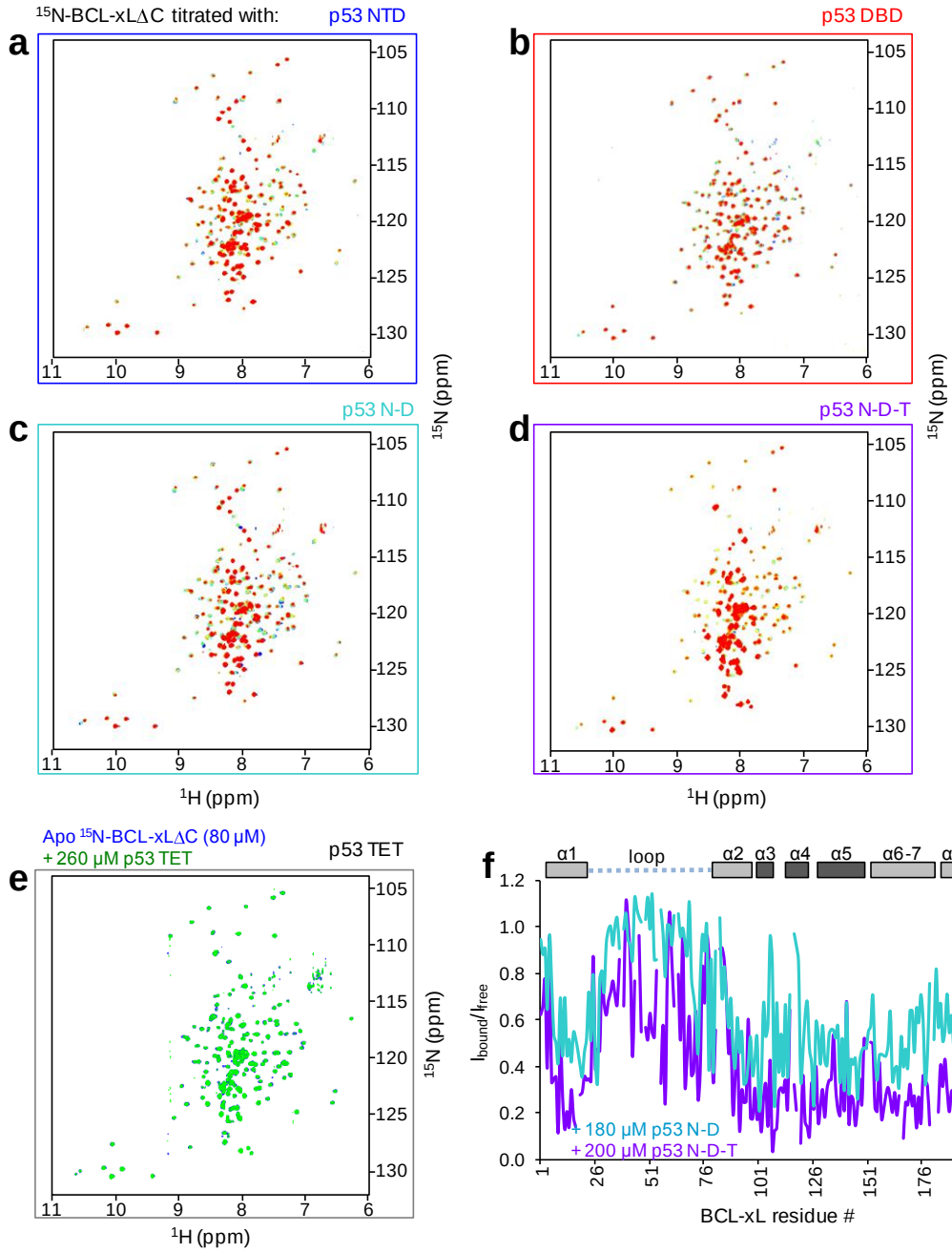

Supplementary Figure 1. NMR Titrations between ^{15}N-BCL-xLΔC and unlabeled p53 domains. Overlaid full views of ^{1}H-^{15}N-TROSY spectra of ^{15}N-BCL-xLΔC upon titration of unlabeled p53 NTD (**a**); p53 DBD (**b**); p53 N-D (**c**); p53 N-D-T (**d**); p53 TET (**e**). For panels **a** trough **d** the displayed spectra follow a blue to red transition color scheme at increasing p53 molar ratios. ^{15}N-BCL-xLΔC concentration was 100 μM in all titrations (80 μM in **e**); p53 NTD (**a**) and p53 DBD (**b**) concentrations were 0, 10, 20, 40, 75, 110, 150, 200, 250, 300 μM; p53 N-D (**c**) concentrations were 0, 10, 25, 50, 75, 120, 180, 250, 300 μM; p53 N-D-T (**d**) concentrations were 0, 10, 25, 50, 75, 110, 150, 200 μM. **f.** Sequence plot of BCL-xLΔC resonance intensities relative to its free state in the presence of 180 μM p53 N-D (green trace) or 200 μM p53 N-D-T (purple trace).

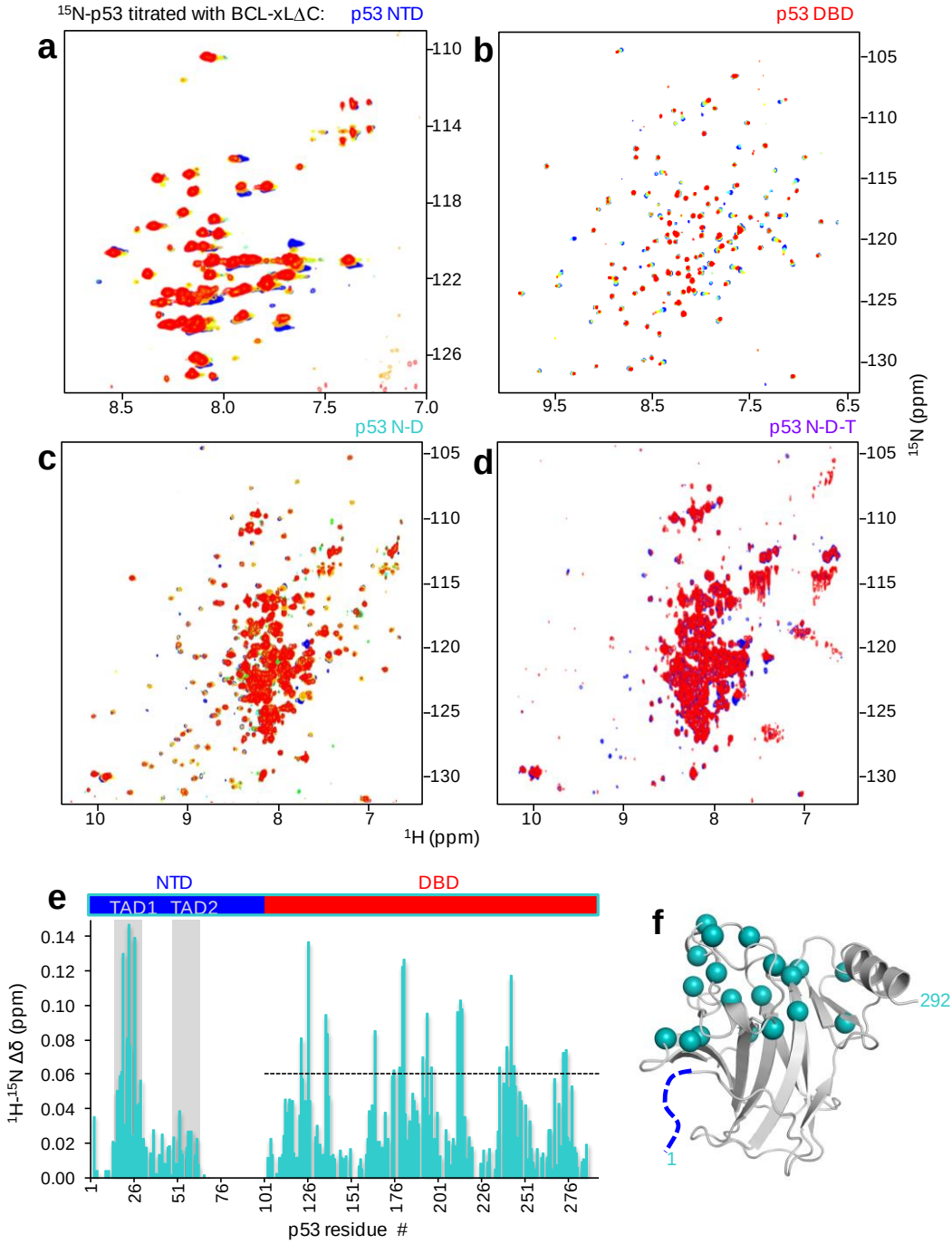

Supplementary Figure 2. ^{1}H-^{15}N-TROSY titrations of unlabeled BCL-xLΔC into various ^{15}N-labeled p53 constructs. Titration of p53 NTD (**a**); p53 DBD (**b**) p53 N-D (**c**) p53 N-D-T (**d**). The displayed spectra follow a blue to red transition color scheme at increasing BCL-xLΔC molar ratios. The concentration of p53 NTD, p53 DBD and p53 N-D was 100 μM; that of p53 N-D-T 180 μM. BCL-xLΔC was titrated into ^{15}N-p53 NTD (**a**) at 0, 50, 100, 200 μM; into ^{15}N-p53 DBD (**b**) at 0, 25, 50, 100, 200, 300 μM; into p53 N-D (**c**) at 0, 25, 50, 100, 150, 200 μM; into p53 N-D-T (**d**) at 0 and 360 μM. **e.** Sequence plot of chemical shift perturbations detected in p53 N-D in the presence of 200 μM BCL-xLΔC. **f**. Mapping of the data displayed in panel **e** onto the p53 DBD structure indicating residues that showed backbone amide chemical shift perturbation > 0.06 ppm.

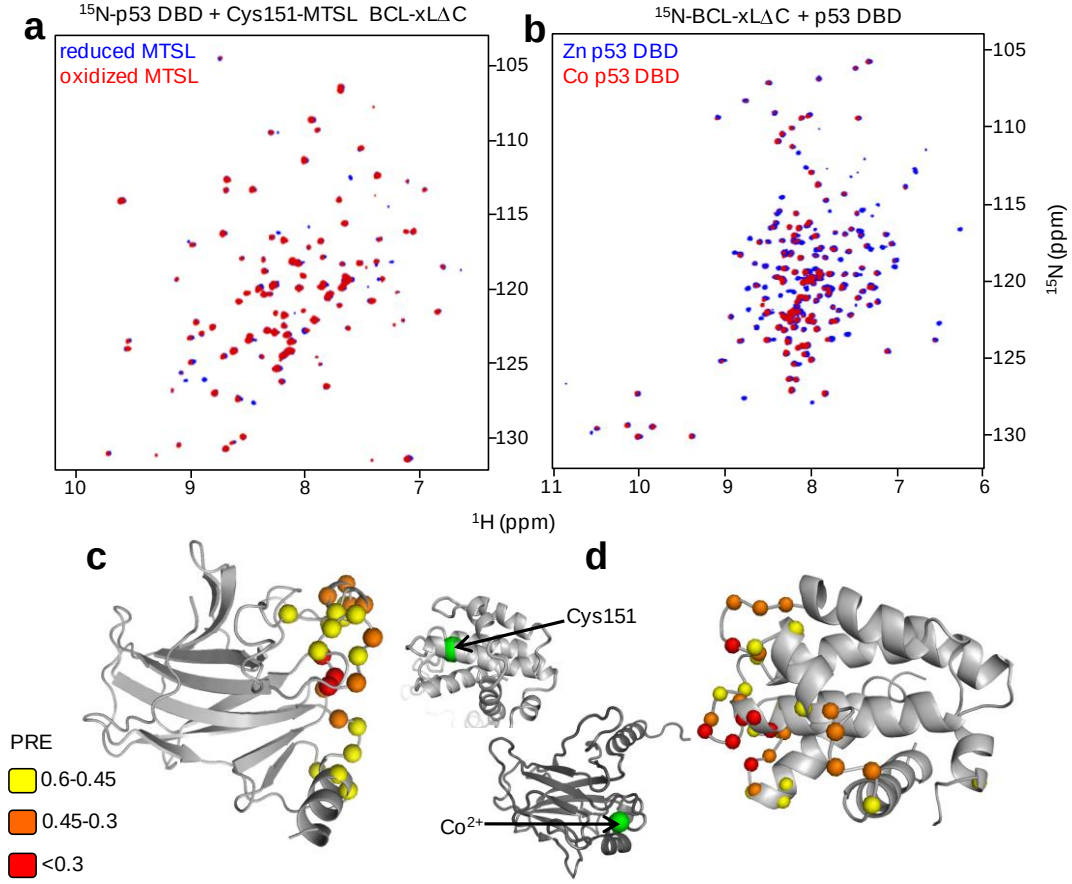

Supplementary Figure 3. Measurements of paramagnetic relaxation enhancements (PREs) for BCL-xLΔC – p53 DBD complex structure determination. **a.** Overlaid ^{1}H-^{15}N-TROSY spectra of ^{15}N-p53 DBD (100 μM) in the presence of reduced (blue) or oxidized (red) Cys151-MTSL labeled BCL-xLΔC (150 μM) and (**b**) of ^{15}N-BCL-xLΔC (100 μM) in the presence of Zn^{2+} (blue) or Co^{2+}-coordinating (red) p53 DBD (150 μM). **c.** Mapping onto the structure of p53 DBD of the paramagnetic relaxation enhancements (PREs) observed in **a**. **d**. Equivalent mapping of PREs observed in **b** onto the structure of BCL-xL.

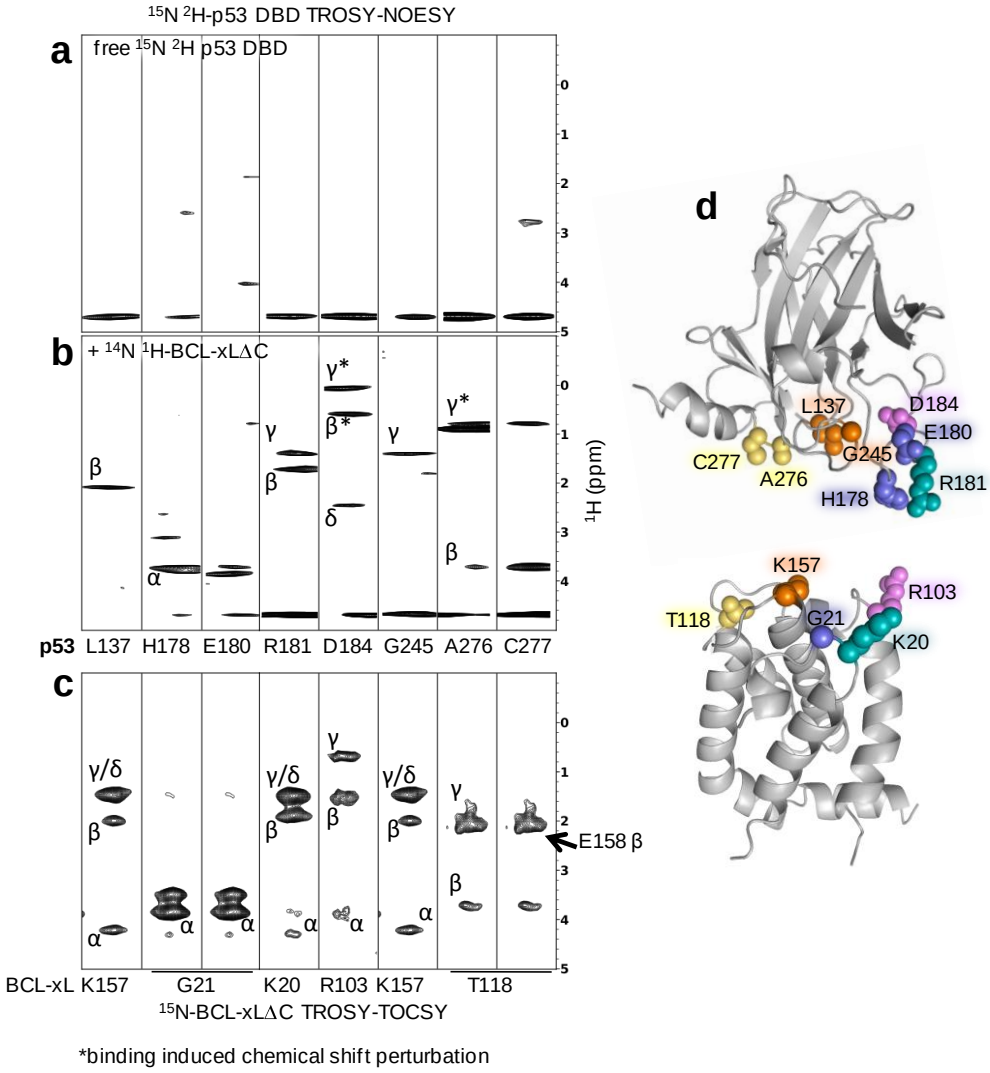

Supplementary Figure 4. Intermolecular NOEs observed between $^{2}H/^{15}N$-p53 DBD and BCL-xLΔC at long NOE mixing time (160 ms). The top two panels display slices of the ^{1}H-^{15}N-TROSY-NOESY 3D spectrum for selected resonances of $^{2}H/^{15}N$-p53 DBD (450 μM) in the absence (**a**) and presence (**b**) of BCL-xLΔC at a 2:1 molar ratio. The bottom panel (**c**) displays slices of the ^{1}H-^{15}N-TROSY-TOCSY spectrum of free ^{15}N-BCL-xL for the residues to which the observed inter-molecular NOEs were assigned. The inter-molecular NOESY peaks in the 3D NOESY spectrum were assigned by inference, with reference to the ^{15}N-TROSY-TOCSY spectrum of free ^{15}N-BCL-xL and with knowledge of preliminary structures based upon extensive PRE data. In a few cases, there are p53 binding-induced chemical shift changes between the two spectra (marked with an asterisk). **d**. Structure mapping of the p53 DBD (top) and BCL-xL (bottom) residues that exhibited intermolecular NOEs shown as spheres and color coded based on their reciprocal assignment.

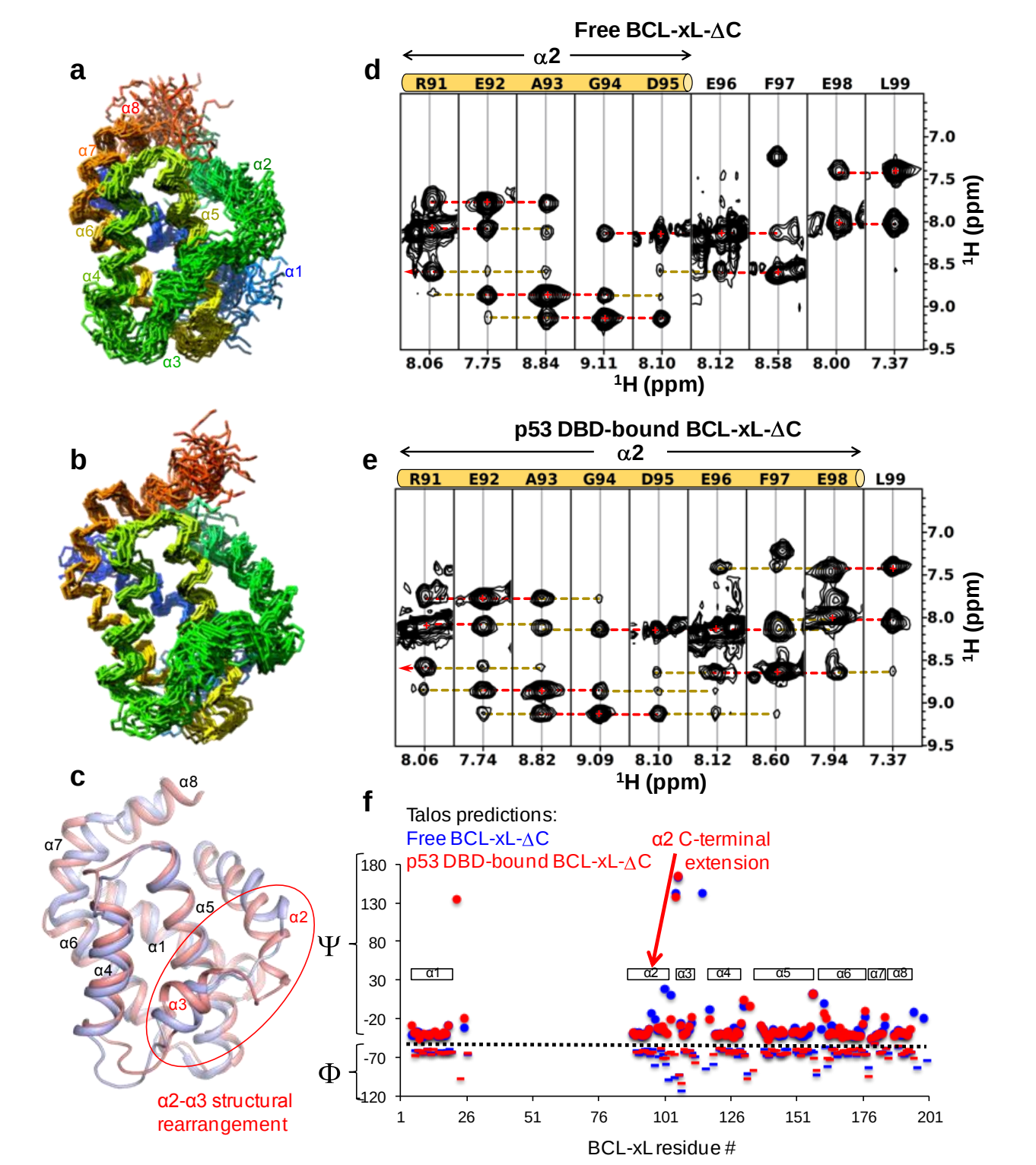

Supplementary Figure 5. Conformational rearrangements take place within BCL-xL upon complex formation with p53 DBD. **a.** Bundle of 20 lowest energy structures of apo BCL-xLΔC calculated with restraints obtained from $^{2}H/^{13}C/^{15}N$-BCL-xLΔC with selective ^{1}H-labeling of Isoleucine, Leucine, Valine methyl moieties. **b.** Equivalent representation of the BCL-xLΔC structure obtained from an identically labeled sample in the presence of p53 DBD. **(continued on the next page)**

Supplementary Figure 5 (continued). c. Overlay between the lowest energy structures in panels **a** (cyan) and **b** (pink). Flexible regions are omitted for clarity. A marked rearrangement of the α2-3 region of BCL-xL is observed upon binding of p53 DBD (highlighted with a red ellipse). **d,e.** Slices corresponding to the C-terminus of α2 of from the ^{1}H-^{15}N-TROSY-NOESY 3D spectrum of ^{2}H/^{13}C/^{15}N-BCL-xLΔC with selective ^{1}H-labeling of Isoleucine, Leucine, Valine methyl moieties in its apo form (**d**) and in the presence of p53 DBD (**e**) highlighting the subtle changes in local stabilization of α-helical structure that takes place in this region of BCL-xL upon binding of p53 DBD. Patterns of NOE cross-peaks indicative of α-helical structure are highlighted by dashed lines (red: i - i 1; yellow: longer range) and the approximate limits of strong α-helical NOE patterns are marked at the top of each panel along with residue labels. All samples contained each protein component at 600 μM. **f.** Sequence mapping of chemical shift-derived backbone dihedral restraints (calculated with the program Talos)[58] for apo BCL-xLΔC (blue) and BCL-xLΔC bound to p53 DBD (red). The position of individual α-helices is marked above the plot. An increase in α-helical dihedral angles is observed at the C-terminus of α2 when BCL-xL is bound to p53-DBD.

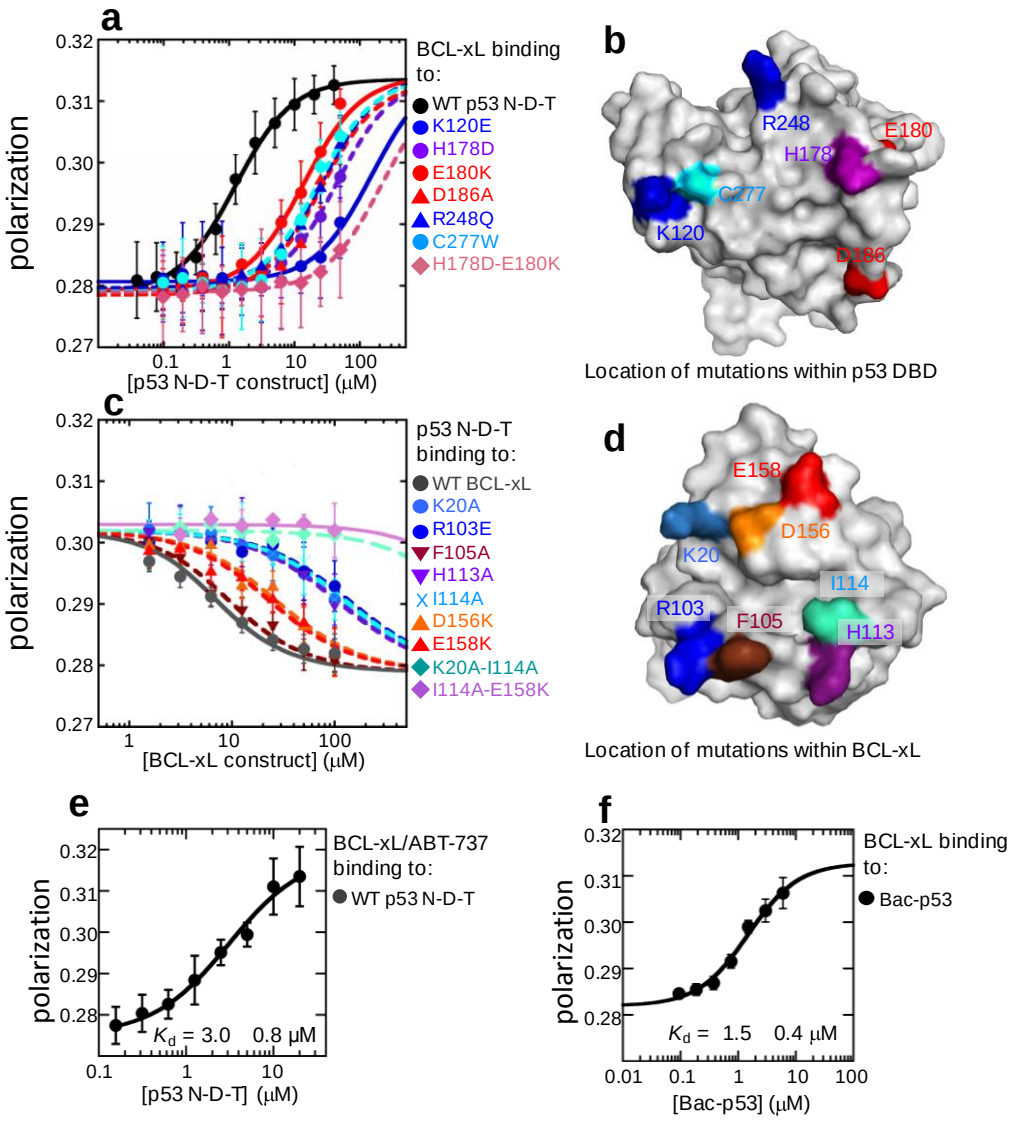

Supplementary Figure 6. Structure based mutagenesis of interfacial residues within the p53 DBD-BCL-xL complex. **a.** Binding titrations between fluorescently labeled, wild-type BCL-xLΔC (F-BCL-xLΔC) and wild-type or mutated p53 N-D-T. Error bars, s.e.m. (n = 3 titrations). **b.** Mapping of the studied mutations on the p53 DBD surface depicted in the same orientation as Figure 4c. **c.** Competition experiments between F-BCL-xLΔC and unlabeled wild-type or mutated BCL-xLΔC for p53 binding. Error bars, s.e.m. (n = 3 titrations). **d.** Mapping of the studied mutations on the BCL-xL surface depicted in the same orientation as Figure 4d. **e.** Fluorescence polarization titration between F-BCL-xLΔC, pre-incubated with 1mM ABT-737 and p53 N-D-T. Error bars, s.e.m. (n = 3 titrations). **f.** Fluorescent polarization titration between F-BCL-xLΔC and full-length, wild-type human p53 expressed from Sf9 insect cells using a Baculovirus expression system (Bac-p53). Error bars, s.e.m. (n = 3 titrations). The measured binding affinity between these two proteins is equivalent to that between F-BCL-xLΔC and the p53 N-D-T bearing core stabilizing mutations.

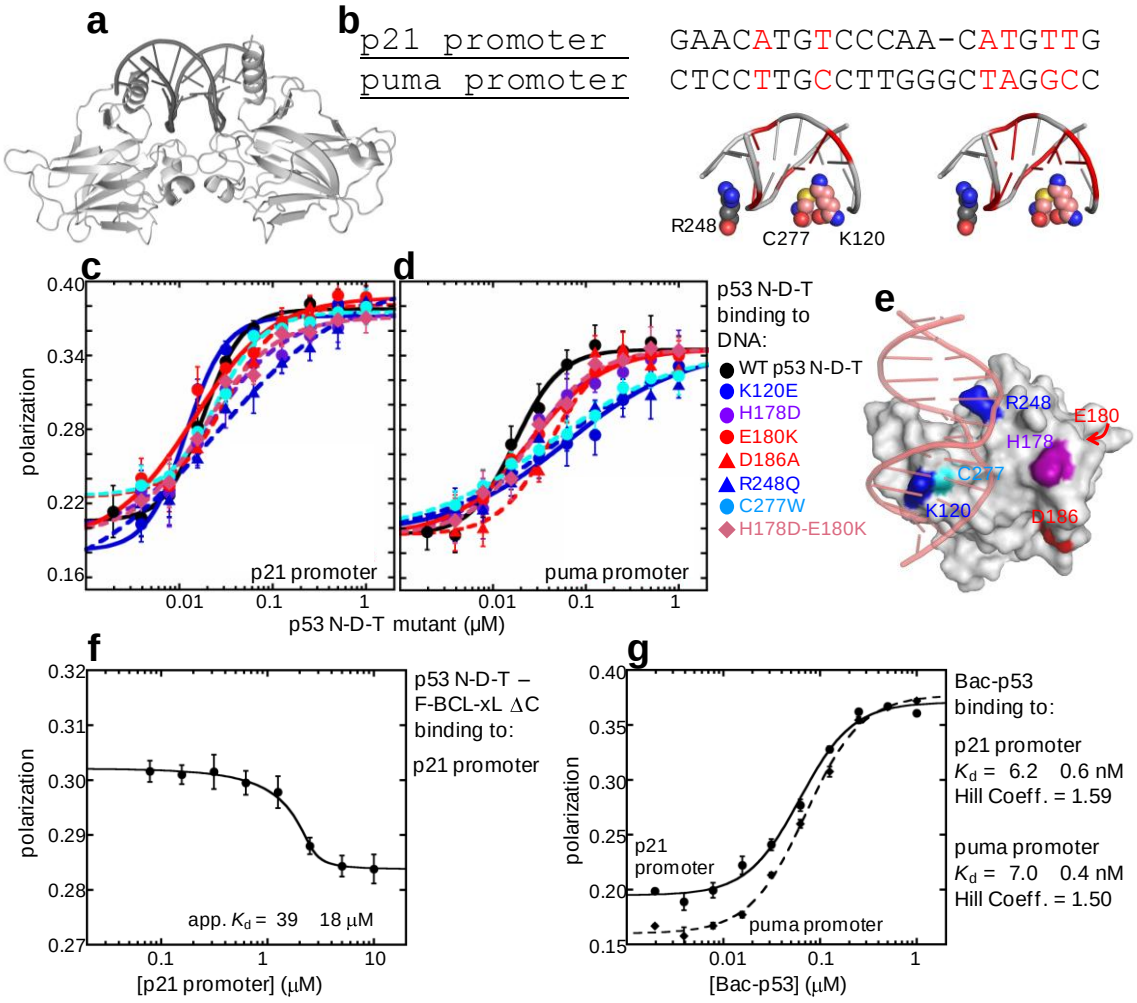

Supplementary Figure 7. Binding titrations between fluorescently labeled, double stranded oligonucleotides and wild-type or mutant p53 N-D-T. **a**. Binding mode between p53 DBD (light grey) and DNA. The minimal binding unit is composed of one double stranded consensus sequence and two p53 DBD. Promoter regions in p53 target genes contain two closely spaced consensus sequences and are bound by p53 tetramers (in a 'dimer of dimers' fashion). **b**. Sequences of the studied oligonucleotides. The partial consensus segments are highlighted in bold characters in each sequence and nucleotides that differ between the two promoters are highlighted in red. The structural depictions at the bottom illustrate how sequence differences between the promoter regions correlate with residues within p53 whose mutation differentially altered the binding affinity for the two promoters. **c**. Fluorescence polarization binding titrations between wild-type or mutant p53 N-D-T and fluorescent p21 promoter. **d**. Analogous representation of binding titrations to the puma promoter. **e**. Structure representation of p53 bound to DNA highlighting interface regions and mutated residues that overlap with the p53 – BCL-xL binding interface. **f.** Competition experiments between F-BCL-xLΔC and an unlabeled p21 promoter double stranded oligonucleotide for p53 binding. **g.** Fluorescence polarization titrations between Bac-p53 and fluorescently labeled DNA. Bac-p53 or p53 N-D-T display comparable binding affinities *in vitro* to these two oligonucleotides. Data in panels **c**,**d**,**f**,**g** represent the average of three independent titrations, error bars indicate s.e.m.

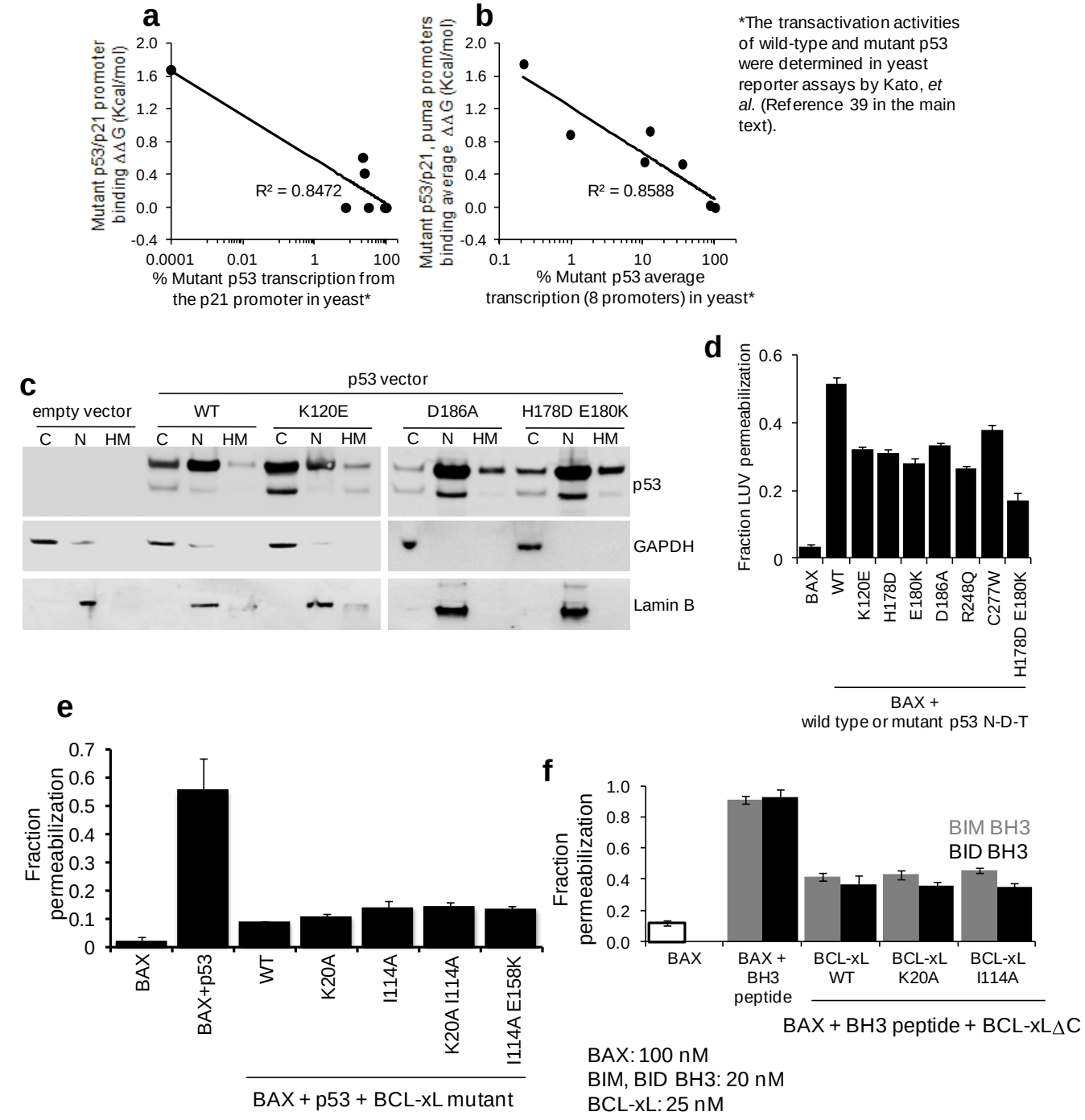

Supplementary Figure 8. Functional relevance of p53 mutations. **a.** Correlation between p21 promoter binding free energies and p21 transcription levels in yeast, as assessed by Kato et al.[39], by wild-type and mutant p53. **b.** Equivalent analysis for the average DNA binding free energies (p21, puma promoter) and the average transcription levels in yeast of all eight p53 target genes analyzed by Kato et al.[39]. **c.** Western blot analysis of cytosolic (C), nuclear (N) and heavy membrane (HM) H1299 cell fractions transfected with empty vector or the indicated p53 constructs. Membranes were probed for p53, Glyceraldehyde 3-phosphate dehydrogenase (GAPDH, cytosolic marker) and Lamin B (nuclear marker). **(continued on the next page)**.

Supplementary Figure 8 (continued). d. Effect of p53 mutations on its ability to activate BAX *in vitro* in a large unilamellar vesicle (LUV) permeabilization assay, analogous to the one reported in Figure 7a d but in the absence of BCL-xL inhibiting BAX activation. All tested mutants induced lower BAX activation compared to wild-type p53, indicating a possible overlap of interaction interfaces between BCL-xL or BAX and p53. Reduction in BAX activation was particularly pronounced for the H178D E180K double mutant, and roughly equivalent to the additive detrimental effect of each individual mutation. **e**. LUV permeabilization assay testing the ability of wild-type or mutant BCL-xLΔC to prevent liposome permeabilization by active BAX. Unlike the one displayed in Figure 7a, in this assay no agent was introduced to block the BH3 binding groove of BCL-xL (BAD BH3, ABT-737) therefore only limited LUV permeabilization was observed in the presence of wild-type or mutant BCL-xLΔC, likely because all these BCl-xL constructs are capable of sequestering partially active BAX by binding its exposed BH3 domain. **f.** LUV permeabilization assay testing the ability of wild-type or mutant BCL-xLΔC to prevent BAX activation by BIM or BID BH3 constructs. In this experiment, BIM-BID BH3 peptides or BIM-BID BH3-BCL-xL complexes were added to LUV samples at a lower concentration than the total amount of BAX present, therefore minimizing any potential effect of BCL-xL sequestration of active BAX. Both tested BCL-xL mutants showed equal ability to the wild-type protein to inhibit BIM-BID-dependent BAX activation.

Fig 6a, p53

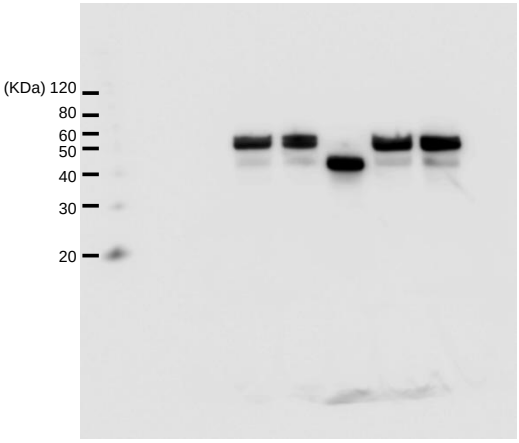

Fig 6a, BCL-xL (p53 co-IP)

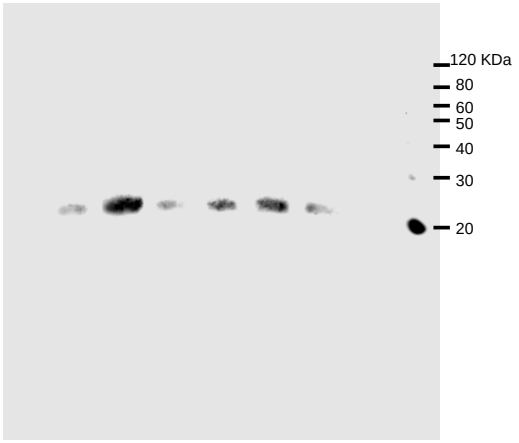

Fig 7e, total p53

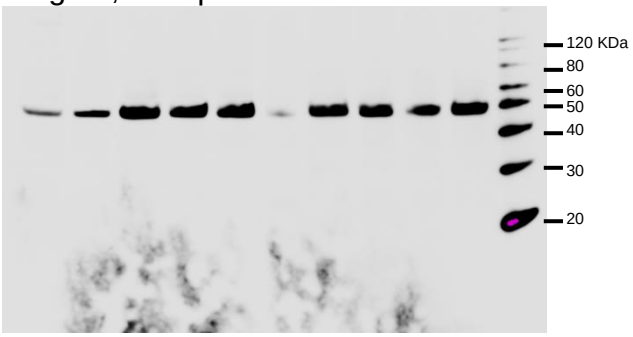

Fig 7e, total BAX

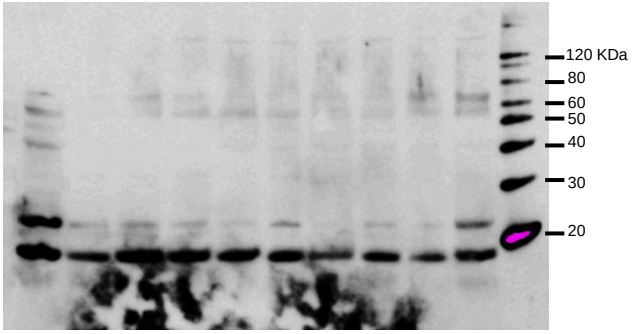

Fig 7e, total Cerulean-BCL-xL

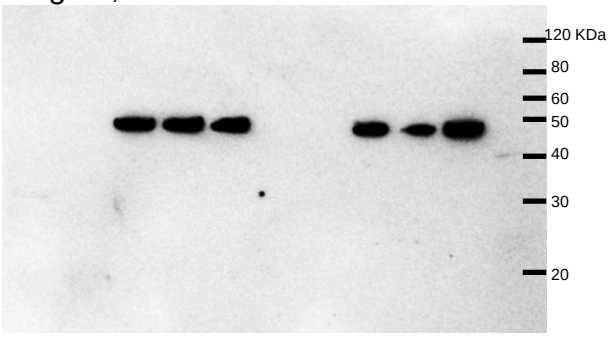

Fig 7e, p53 (Cer-BCL-xL co-IP)

Fig 7e, BAX (Cer-BCL-xL co-IP)

Supplementary Figure 9. Full images of western blots displayed in cropped format in Figures 6 and 7

Supplementary Table 1. Average thermodynamic parameters extracted from duplicate ITC titrations of BCL-xLΔC into p53 NTD or BCL-xLΔLΔC into p53 DBD, p53 N-D, p53 D-T and p53 N-D-T.

	p53 construct					
	NTD	DBD	TET	N-D	D-T	N-D-T
N	1*	1*	N.D.	1*	0.95±0.02	1.0±0.1
K_D (μM)	250±80	17±2	N.D.	30±20	1.9±0.1	0.6±0.3
ΔH (Kcal/mol)	-4.4±0.2	-2.1±0.2	N.D.	-0.9±0.2	-1.43±0.03	-2.0±0.2
-TΔS (Kcal/mol)	-0.6±0.3	-4.5±0.3	N.D.	-5.1±0.6	-6.38	-6.5±0.6
ΔG (Kcal/mol)	-5.0±0.5	-6.6±0.5	N.D.	-6.0±0.8	-7.8	-8.5±0.8

Error values indicate s.e.m.

SUPPLEMENTARY NOTE

1. SUPPLEMENT TO ONLINE METHODS

Reagents

All gene constructs for bacterial expression were cloned into pET28 plasmid (EMD Biosciences) encoding for a hexa-histidine affinity tag separated from the N-terminus of the protein construct by a Thrombin digestion site. Construct containing the p53 DBD sequence included the following core stabilizing mutations: M133L, V203A, N268D[28]. Other mutations in both p53 and BCL-xL constructs were introduced with a QuickChange II-Gold site-directed mutagenesis kit (Quiagen) according to the manufacturer protocol, primer DNA was synthesized by the Hartwell Center for Bioinformatics and Biotechnology (HC) at SJCRH or International DNA Technologies Inc. DNA purification was performed with Miniprep, Maxiprep (Invitrogen) or Zyppy Plasmid Miniprep kit (Zymo Research). DNA sequencing was performed by the Hartwell Center for Bioinformatics and Biotechnology. The BID (sequence QEDIIRNIARHLAQVGDSMDRSIPP), BIM (sequence DNRPEIWIAQELRRIGDEFNAYYAR), BAD (sequence NLWAAQRYGRELRRMSDEFVDSFKK) and BAX (sequence PQDASTKKSECLKRIGDELDSNMEL) peptides were synthesized by the HC using standard solid-phase FMOC-based synthesis with N terminal acetylation and C terminal amidation. The crude products were HPLC purified to >98% purity. Full length, wild-type human p53 expressed in Sf9 insect cells by Baculovirus transfection was purchased from ProteinOne (catalog number: P2001).

Protein expression and purification

All proteins were expressed in E. coli BL21(DE3) expression strain. Unlabeled proteins were expressed in LB media, isotopically labeled ones in MOPS minimal media supplemented with the appropriate labeling reagents dissolved in H_2O or D_2O. Selective protonation of Isoleucine, Leucine, Valine methyl moieties was performed according to established procedures[53]. Culture media were generally grown at 37°C until their optical density at 600 nm (OD_{600}) reached a value of 0.6, then induced with 0.5 mM IPTG for 5 hours at 37°C and harvested. For expression of constructs containing p53 DBD, the media was cooled to 20°C, supplemented with 0.2 mM $ZnSO_4$ or $CoSO_4$ 30' prior to IPTG induction, which was carried on for 16 hours at 20°C. BCL-xL-expression cells were lysed by osmotic choc in a buffer containing 25 mM Tris, 500 mM NaCl, 5 mM imidazole, 20% w/v sucrose, 1 mg/mL lysozime, pH 8.0. The soluble fraction of the lysate was then purified by Ni affinity chromatography followed by cleavage of the 6xHis tag with restriction grade thrombin (Novagen) and anion exchange chromatography using mono-dispersed Q –sepharose resin. This step allows for a complete resolution of native monomeric, loop deamidated and dimeric BCL-xL obtained after the Ni affinity step. The whole purification procedure was performed in Tris buffer with either imidazole or NaCl gradient and pH 8.0 or 7.0 for the Ni-affinity or anion exchange step respectively. For the purification of p53 NTD, cell pellets were lysed with a microfluidizer in 25 mM Tris, 500 mM NaCl, 5 mM imidazole, pH 8.0. The supernatant was purified by Ni affinity chromatography followed by thrombin cleavage of the 6xHis tag, removal of the cleaved peptide on Ni-NTA resin and a final boiling purification step. Cell pellets containing expressed p53 DBD, D-T and N-D-T constructs were lysed by sonication in 50 mM potassium phosphate, 300 mM NaCl, 2 mM TCEP, 1 mg/mL lysozime, pH 8.0, followed by Ni-affinity purification in 25 mM Hepes, 0.5 M NaCl, 2 mM TCEP, pH 7.0 with an imidazole gradient. The elution fractions were dialyzed against 25 mM Bis-Tris propane, 50 mM NaCl, 5 mM DTT, pH 6.5 buffer and thrombin cleaved, followed by a Heparin affinity purification step with NaCl gradient. To maximize the yield, the insoluble fraction of isotopically labeled $^{2}H/^{13}C/^{15}N$-p53 N-D-T was recovered from inclusion bodies and refolded according to an established procedure[54], then purified as above. The p53 N-D construct was similarly purified in Tris buffers with the Heparin affinity step being replaced by anion exchange on Q-sepharose. All purified proteins were concentrated on Centricon devices, flash frozen and stored at -80 °C. The tetramerization domain of p53 (TET) was purified according to established procedures[30]. Monomeric, full length human BAX, bacterially expressed from a pTYB1 vector (New England Biolabs) as a self-cleavable intein – chitin binding protein fusion construct, was purified according to established procedures[29]. Protein concentrations were determined by measuring absorbance at 280 nm after dilution in 6M guanidinium hydrochloride. Extinction coefficients were obtained using the ProtParam tool (www.expasy.org/protparam).

NMR Spectroscopy

Resonance assignments were derived from published assignments of each studied construct, confirmed and integrated with HNCA, HNCACB, HNCO, HNcoCA and ^{15}N-edited TROSY-NOESY 3D experiments for p53 DBD; with HNCA, HNCACB, HNCO (for assignment of CBCACO spectra), ^{15}N-edited TROSY-NOESY and ^{15}N-edited TROSY-TOCSY for free BCL-xLΔC. ^{15}N-edited TROSY-NOESY spectra were used for the assignment of BCL-xLΔC bound to unlabeled p53 DBD. HCC-TOCSY and ^{13}C-edited HSQC-NOESY were employed for assignment of Isoleucine, Leucine, Valine side chain methyl resonances in proteins with selective methyl labeling. NOESY cross peaks from ^{15}N and ^{13}C-edited NOESY spectra were employed for the structural calculations described below. 3D experiments were typically collected for 16-48 scans, depending on sample concentration and experiment sensitivity, over 2048 x 40-64 x 80-128 points and processed with zero filling and linear prediction of 32 complex points in the indirectly detected dimensions over spectral windows of 14 ppm (^{1}H) 32 ppm (^{15}N), 18 ppm (^{13}C HNCO) 32 ppm (^{13}C, HNCA, HNcoCA), 70 ppm (^{13}C, HNCACB) 95 ppm (^{13}C, HCC-TOCSY) with appropriate offsets. ^{15}N-TROSY spectra were collected over 16 scans, 2048 x 256 points and spectral windows of 14 ppm (^{1}H) x 32 ppm (^{15}N). ^{13}C-HSQC spectra were collected over 8-24 scans, 2048 x 256 points, spectral window of 14 x 30 ppm. 2D CBCACO spectra were collected over 128 scans, 800 x 128 points, spectral window of 18 x 100 ppm. ^{15}N-TROSY and CRINEPT-TROSY spectra of p53 1-360 (180 μM, in 20 mM sodium phosphate, 150 mM KCl, 5 mM DTT, 0.1% NaN_3, pH 7.2) were collected at 20 C over 400 and 256 scans respectively, 2048 x 128-256 points.

Isothermal Titration Calorimetry

Binding between BCL-xL and p53 constructs. BCL-xLΔC or BCL-xLΔLΔC (300 μM or 1 mM) were titrated into solutions containing the various employed p53 constructs at nominal concentrations of 30 or 100 μM. The exact concentration of each sample was verified after dialysis.

Binding of BID BH3 peptide to BCL-xL in the presence of p53 constructs. In these experiments the concentration of BCL-xLΔC (cell) and BID BH3 peptide (syringe) was kept constant in all titrations (5 μM and 50 μM respectively), while that of the different p53 constructs was adjusted to favor their binding to BCL-xL based on our previous knowledge of the various complexes K_ds (p53 NTD: 200 μM; p53 DBD and p53 N-D: 40 μM; p53 D-T and p53 N-D-T: 10 μM).

Binding of BAX, BIM or BID BH3 peptides to wild-type and mutant BCL-xL. each BH3 peptide (100 μM) was titrated into 10 μM solutions of the various BCL-xL constructs under the same conditions described above.

Large unilamellar vesicle assays

The following final concentrations were employed for the various sample components: BAX = 100 nM; p53 N-D-T = 500 nM; BCL-xLΔC – BAD BH3 or BCL-xLΔC – ABT737 complexes = 2 μM). The various BCL-xLΔC constructs (100 μM), were pre-incubated with a 1.2 molar excess of BAD BH3 for 30 minutes before diluting the complex solutions in LUV samples; ABT-737 was diluted from a 10 mM DMSO stock solution to a final concentration of 2 μM in LUV buffer, followed by addition of BAX and BCL-xLΔC before a final addition of p53 N-D-T. To test the protective effect of wild-type and mutant BCL-xL against BAX activation by BIM or BID BH3 peptides, the latter were prepared in 1 μM stocks and pre-mixed with a 1.25 molar excess of wild-type or mutant BCL-xL, then diluted to a final concentration of 20 nM peptide (25 nM BCL-xL) in LUV samples containing 100 nM BAX. These assay conditions therefore prevented undesired inhibition of BAX activation by excess BCL-xL. Each condition was tested in four independent samples.

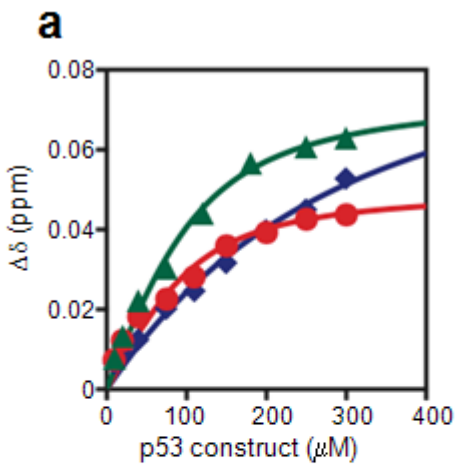

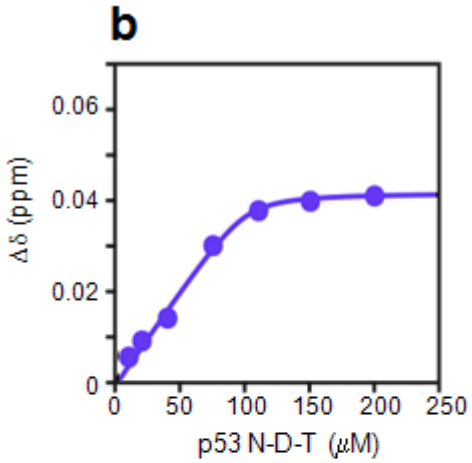

c

domain	# of resonances used in fitting	Fitted K_d (μM)
NTD	13	230 ± 90
DBD	14	30 ± 20
N-D	15	40 ± 10
N-D-T	10	1.2 ± 0.6

Estimates of binding affinities between BCL-xL and p53 constructs from analysis of NMR titrations.
Fitting to a 1:1 binding isotherm of average observed chemical shift perturbation (CSP) within ^{15}N-BCL-xLΔC upon titration of p53 NTD (blue), p53 DBD (red) and p53 N-D (green - **a**); p53 N-D-T (**b**). **c**. Summary of the number of perturbed resonances averaged for each curve fitting and fitted dissociation constant (K_d) values.

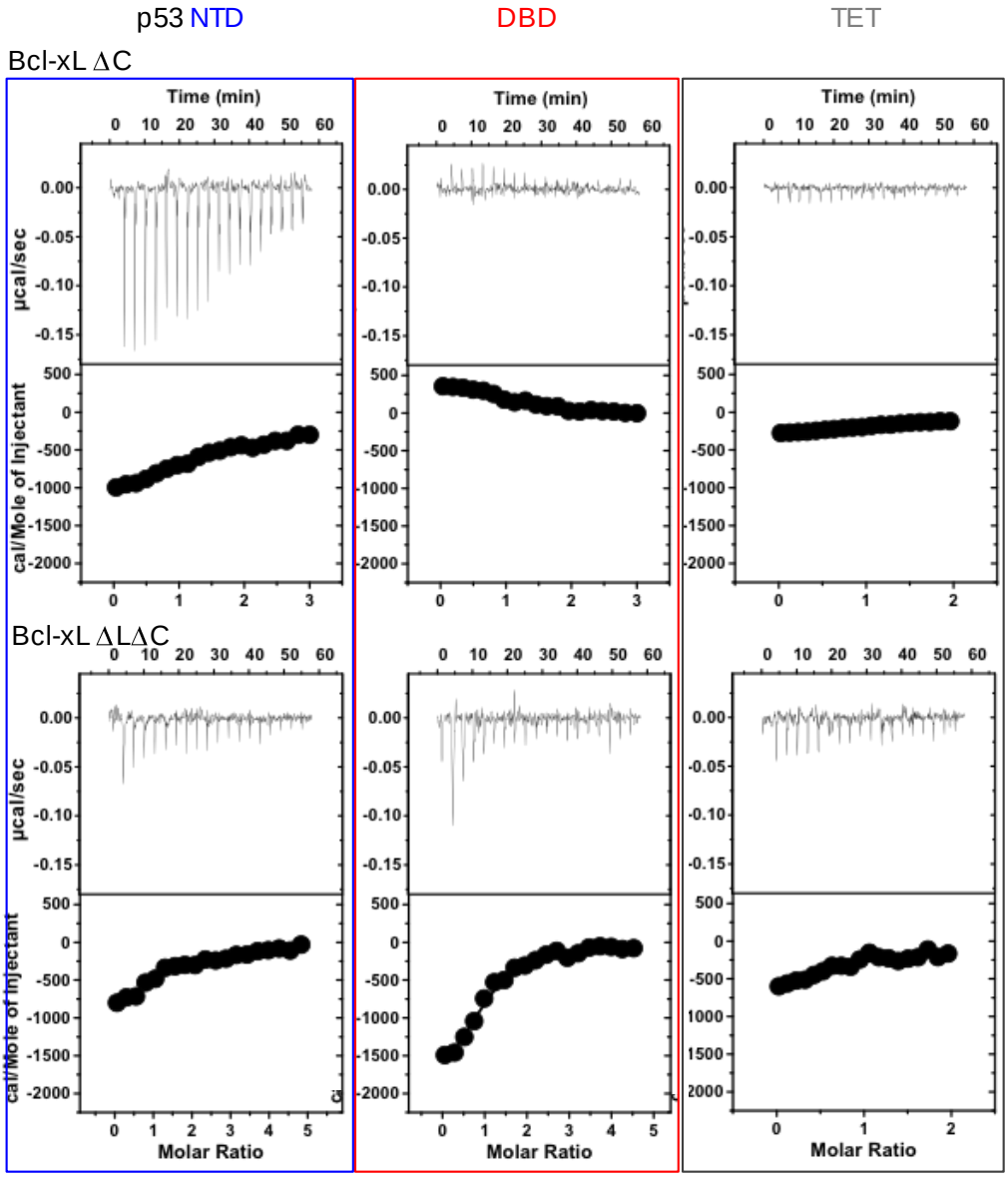

Isothermal titration calorimetry (ITC) thermographs and integrated heat values for titration of BCL-xLΔC (top panels) or BCL-xLΔLΔC (bottom panels) into the various indicated p53 constructs.

Titration of BCL-xLΔC, a construct that contains a large disordered loop between α1 and α2, generally resulted in small, slightly endothermic heat signatures. BCL-xLΔLΔC, which does not contain this loop, displayed exothermic binding to all p53 constructs. We ascribed this difference in binding thermodynamics to a perturbation (increase) of the BCL-xL α1-α2 loop dynamics upon interaction with p53. Due to the extremely small heats observed in BCL-xLΔC titrations, only BCL-xLΔLΔC titrations were employed to extract thermodynamic parameters.

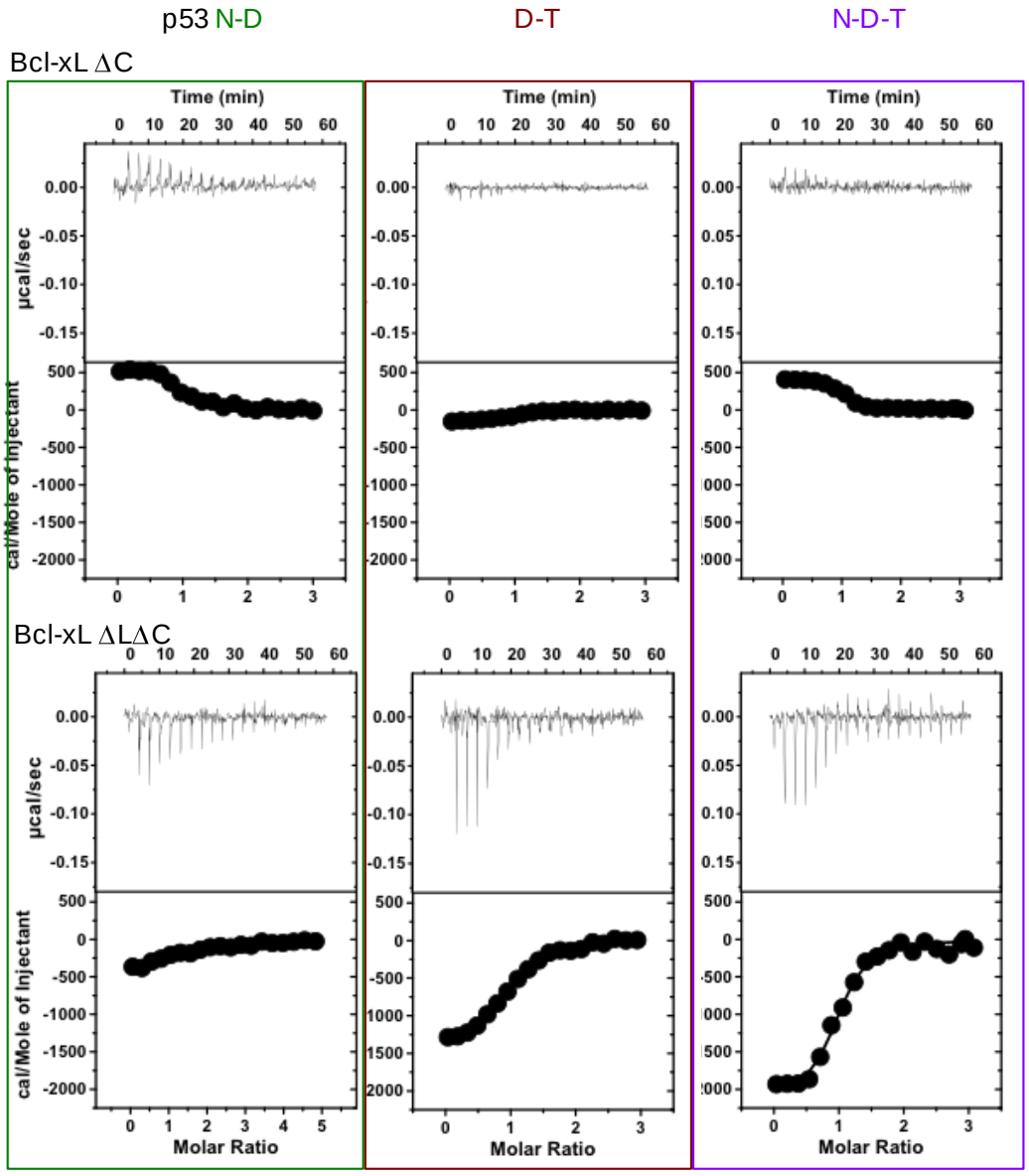

Isothermal titration calorimetry (ITC) thermographs and integrated heat values for titration of BCL-xLΔC (top panels) or BCL-xLΔLΔC (bottom panels) into the various indicated p53 constructs.

Titration of BCL-xLΔC, a construct that contains a large disordered loop between α1 and α2, generally resulted in small, slightly endothermic heat signatures. BCL-xLΔLΔC, which does not contain this loop, displayed exothermic binding to all p53 constructs. We ascribed this difference in binding thermodynamics to a perturbation (increase) of the BCL-xL α1-α2 loop dynamics upon interaction with p53. Due to the extremely small heats observed in BCL-xLΔC titrations, only BCL-xLΔLΔC titrations were employed to extract thermodynamic parameters.

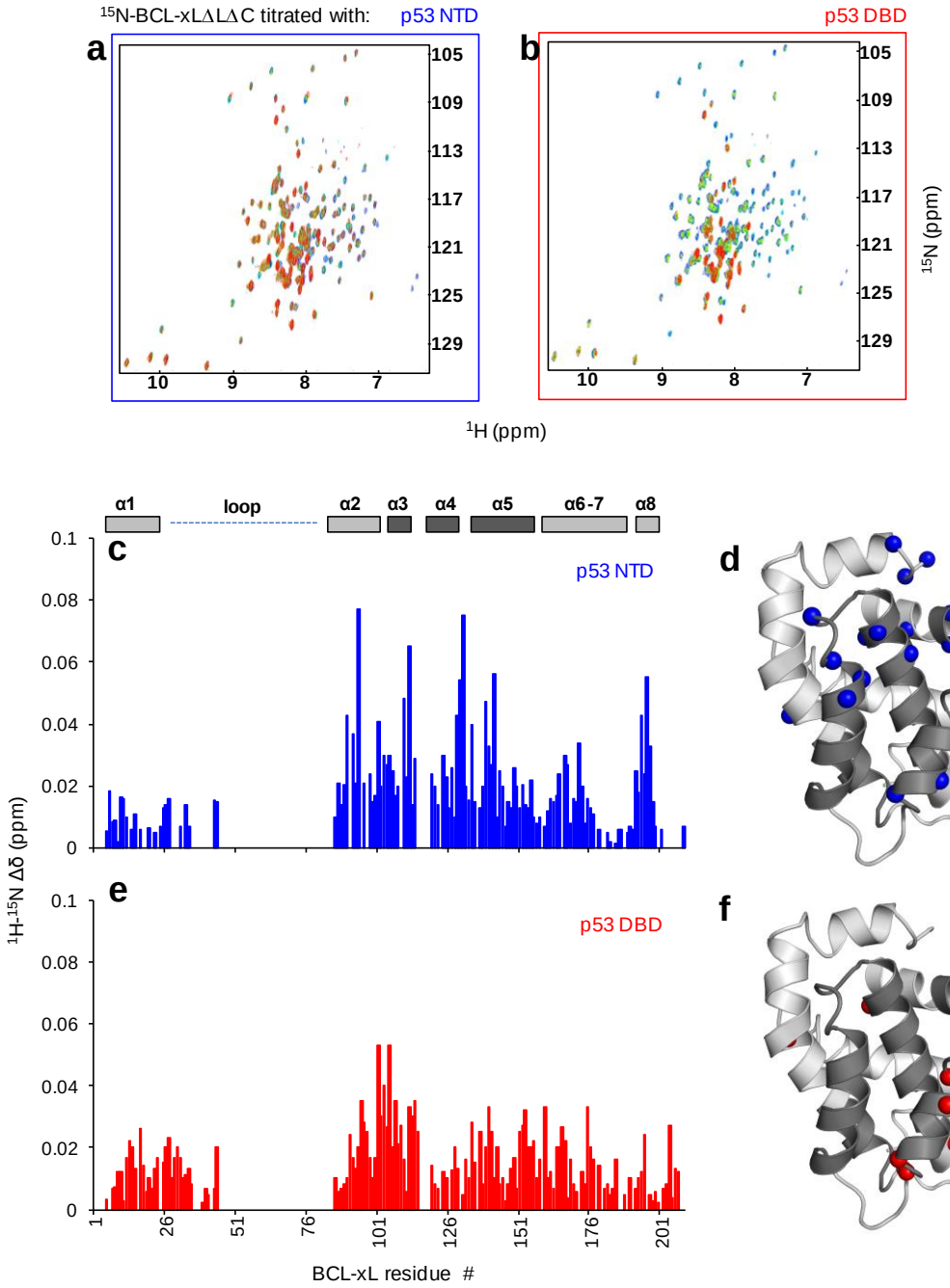

NMR Titrations between loop-truncated BCL-xL construct and individual domain p53 constructs.

^{1}H-^{15}N-TROSY spectra of ^{15}N-BCL-xLΔLΔC upon titration of unlabeled p53 NTD (**a**) or p53 DBD (**b**). The displayed spectra follow a blue to red transition color scheme at increasing p53 molar ratios. The concentration of ^{15}N-BCL-xLΔLΔC was 100 μM in both titrations and either p53 construct was added at 0, 50, 100, 200, 400 μM. **c**. Sequence and (**d**) structure mapping of the chemical shift perturbations observed for ^{15}N-BCL-xLΔLΔC at the highest concentration of p53 NTD. **e**. Analogous sequence and (**f**) structure mapping for the titration of p53 DBD into ^{15}N-BCL-xLΔLΔC. The threshold perturbation value utilized for structure mapping was 0.03 ppm.

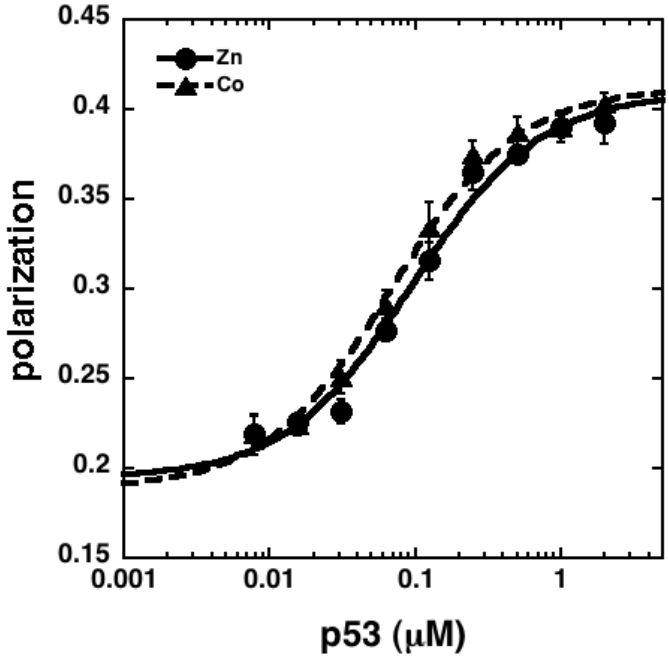

Fluorescence polarization titration of Zn^{2+} or Co^{2+}-coordinating p53 DBD binding to a fluorescein-labeled double stranded consensus oligonucleotide.
The identical ability of the two proteins to bind DNA confirms the proper fold of the Co^{2+} containing construct.

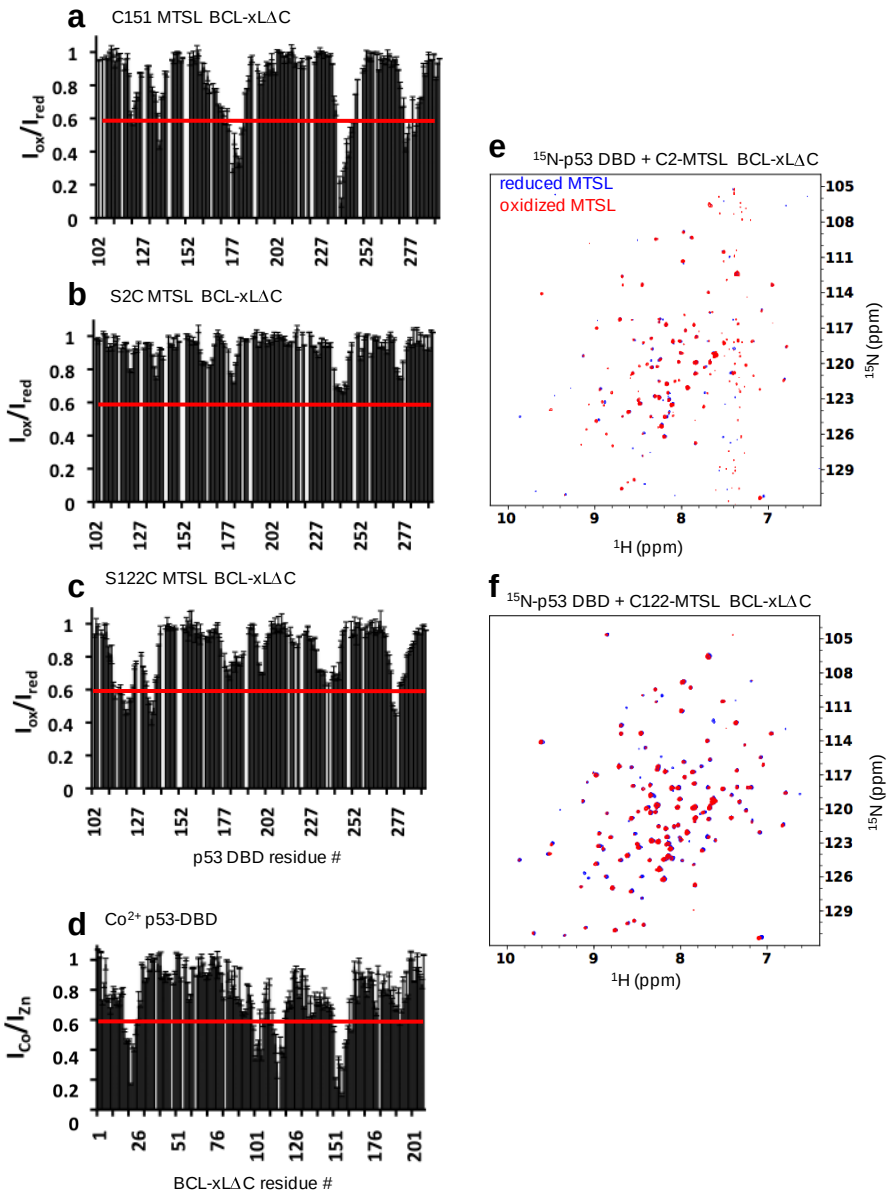

Summary of PRE measurements on backbone amides for structure determination of the BCL-xL – p53 DBD complex.

Sequence mapping of PREs induced in the ^{1}H-^{15}N-TROSY spectrum of ^{15}N-p53 DBD by Cys151-MTSL BCL-xLΔC (**a**), C151S, S2C-MTSL BCL-xLΔC (**b**) and C151S, S122C-MTSL BCL-xLΔC (**c**). **d**. Sequence mapping of PREs observed in the ^{1}H-^{15}N-TROSY spectrum of ^{15}N-BCL-xLΔC in the presence of Co^{2+}-coordinating p53 DBD. Error bars are inversely proportional to the signal to noise ratio of individual resonances. The threshold value (0.6) for the introduction of attractive constraints in structure determination is highlighted by a horizontal red line in all the plots. **e**. Overlaid ^{1}H-^{15}N-TROSY spectra of ^{15}N-p53 DBD (100 μM) in the presence of reduced (blue) or oxidized (red) C151S S2C-MTSL labeled BCL-xLΔC (150 μM). **f**. Overlaid ^{1}H-^{15}N-TROSY spectra of ^{15}N-p53 DBD (100 μM) in the presence of reduced (blue) or oxidized (red) C151S S122C-MTSL labeled BCL-xLΔC (150 μM).

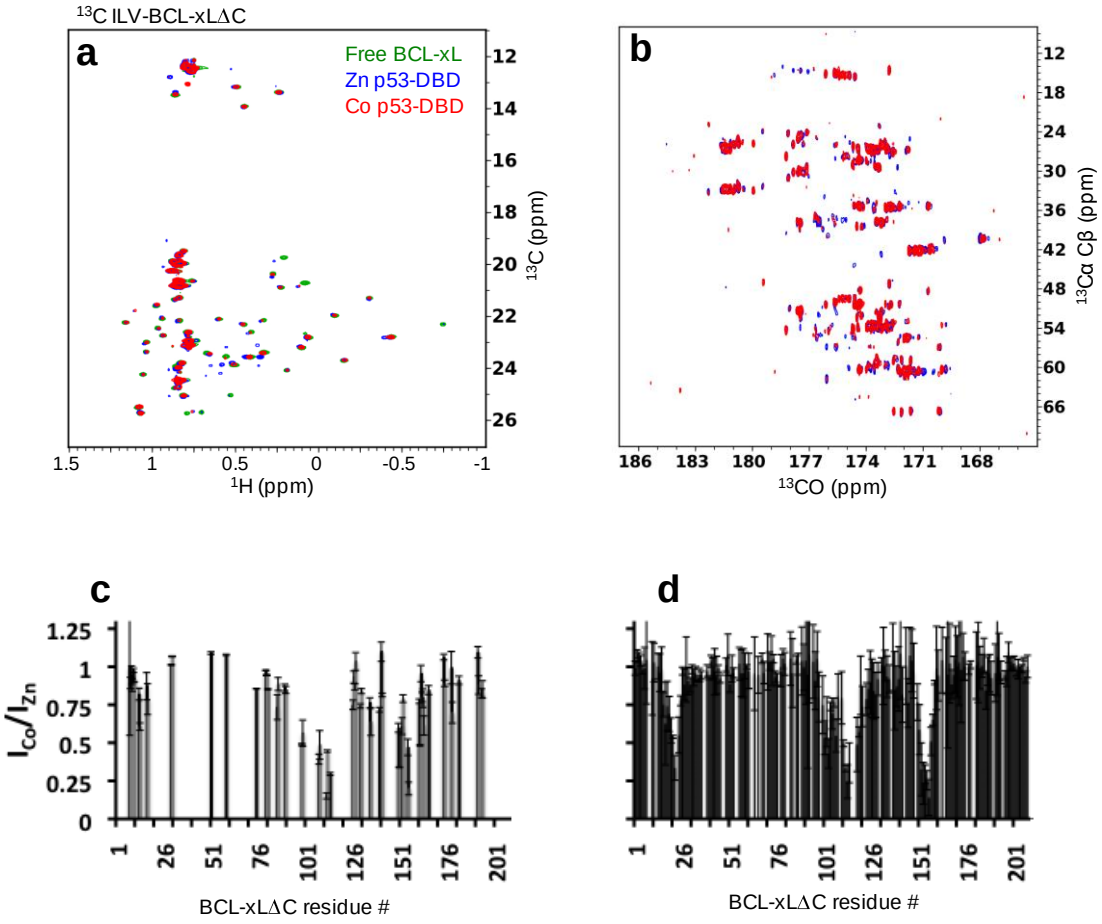

Summary of ^{13}C-detected PRE measurements for structure determination of the BCL-xL – p53 DBD complex.

Overlaid ^{1}H-^{13}C-HSQC (**a**) or CBCACO (**b**) spectra of ^{2}H/^{13}C/^{15}N-BCL-xLΔC with selective ^{1}H-labeling of Isoleucine, Leucine, Valine methyl moieties in its free state (1 mM; green, panel **a** only) and in the presence of Zn^{2+} (blue) or Co^{2+}-coordinating (red) p53 DBD (in equimolar concentration to the labeled BCL-xL component, 600 μM). **c,d**. Mapping of the PREs observed in **a** and **b** respectively onto the BCL-xL sequence.

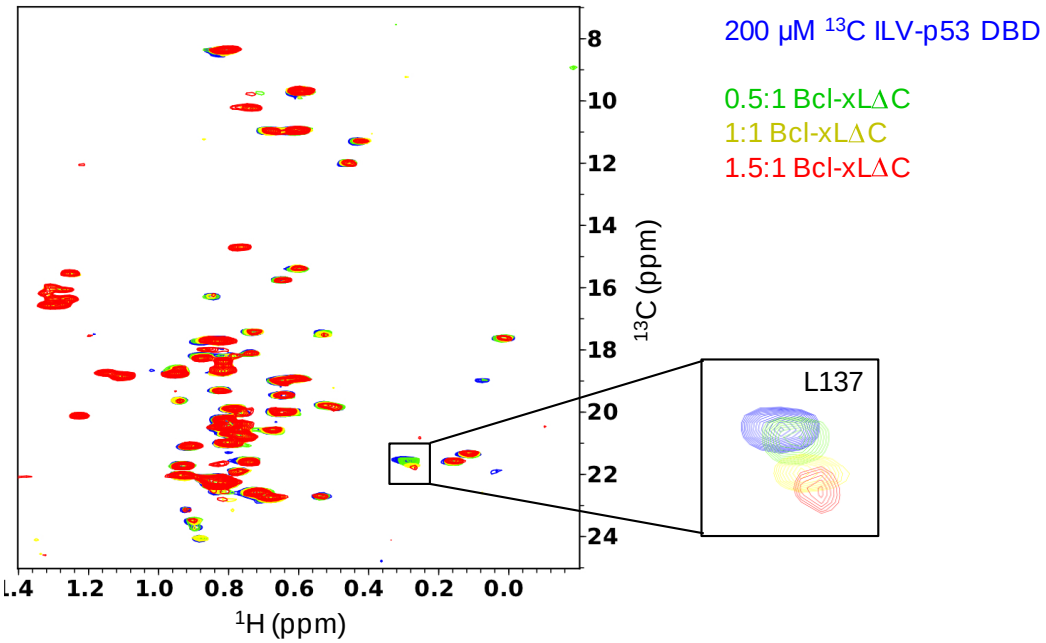

Chemical shift perturbations in aliphatic side-chains of p53 upon titration of BCL-xL.

Overlaid ^{1}H-^{13}C-HSQC spectra of ^{2}H/^{13}C/^{15}N-p53 DBD with selective ^{1}H-labeling of Isoleucine, Leucine, Valine methyl moieties in its free state (200 μM, blue) and upon titration of 100 (yellow) 200 (green) and 300 μM (red) BCL-xLΔC respectively. Due to the scarce presence of hydrophobic residues at the interface between p53 DBD and BCL-xL, only p53 Leu^{137} exhibits noticeable chemical shift perturbation upon addition of BCL-xL.

p53 residue	BCL-xL residue
Electrostatic interactions	
Zn^{2+}	E153; D156
E180	K20
D186	R103
R248	E158
Hydrogen bonds	
K120	Y120; Q121
Q136	I114 backbone
K139	H113 backbone
H179	E98
R181	Q19
C182 backbone	R102
N239	K157
S241	K157 backbone
Hydrophobic patches	
L137; M237; A276	F105; I114; P116; T118
M243	Y22

List of residue pairs or small clusters of residues involved in intermolecular contacts (electrostatic, hydrogen bonds, or hydrophobic) between p53 DBD and BCL-xL.

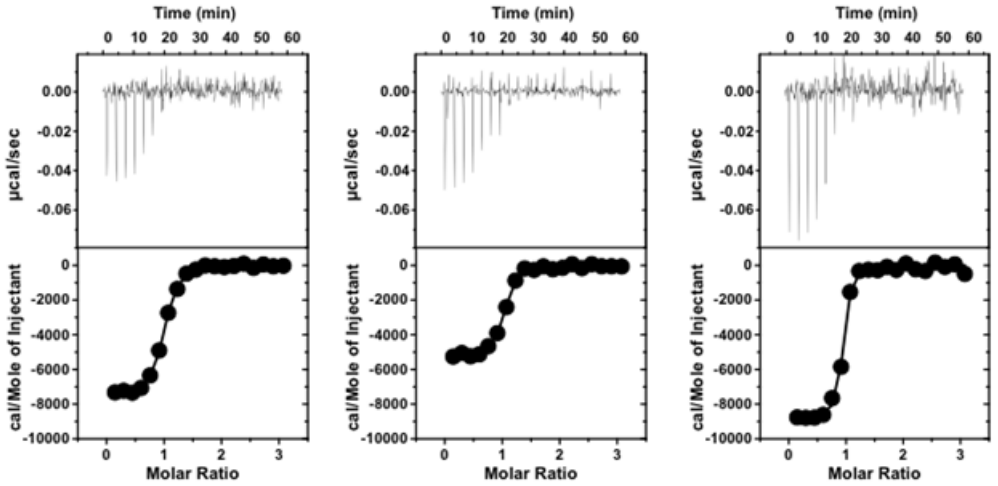

free Bcl-xLΔC
N = 0.97±0.03
K_D= 23±7 nM
ΔH = -8.1±0.6 Kcal/mol
ΔS = +8±1 cal/mol*K
-TΔS = -2.4±0.3 Kcal/mol
ΔG = -10.5±0.2 Kcal/mol

Bcl-xLΔC – p53 NTD
N = 0.93±0.06
K_D= 37±6 nM
ΔH = -5.8±0.5 Kcal/mol
ΔS = +15±2 cal/mol*K
-TΔS = -4.4±0.6 Kcal/mol
ΔG = -10.1±0.1 Kcal/mol

Bcl-xLΔC – p53 DBD
N = 0.91±0.02
K_D= 7±2 nM
ΔH = -8.6±0.3 Kcal/mol
ΔS = +9±1 cal/mol*K
-TΔS = -2.6±0.4 Kcal/mol
ΔG = -11.2±0.2 Kcal/mol

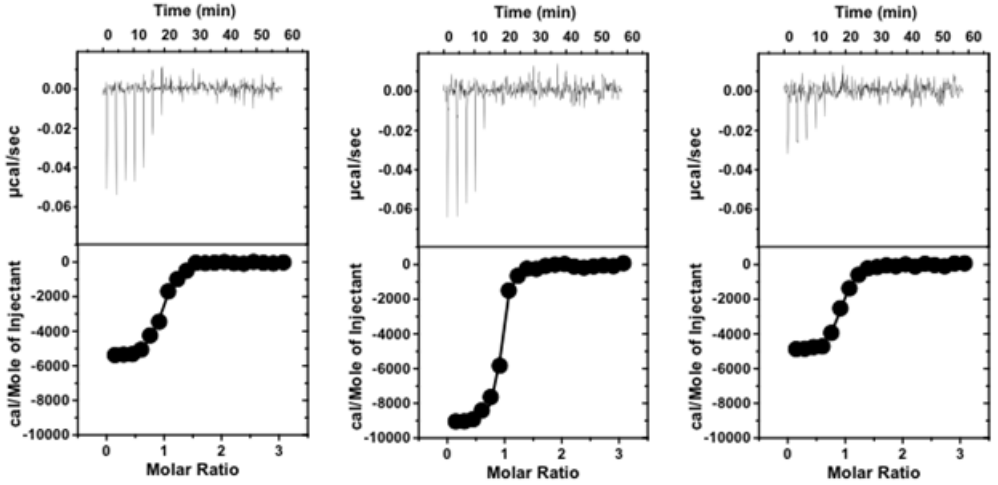

Bcl-xLΔC – p53 NT-DBD
N = 0.93±0.02
K_D= 63±8 nM
ΔH = -5.8±0.3 Kcal/mol
ΔS = +13±1 cal/mol*K
-TΔS = -4.0±0.4 Kcal/mol
ΔG = -9.8±0.1 Kcal/mol

Bcl-xLΔC – p53 DBD-TET
N = 0.885±0.003
K_D= 7±4 nM
ΔH = -9.7±0.7 Kcal/mol
ΔS = +5±1 cal/mol*K
-TΔS = -1.6±0.3 Kcal/mol
ΔG = -11.2±0.3 Kcal/mol

Bcl-xLΔC – p53 1-360
N = 0.89±0.02
K_D= 35±4 nM
ΔH = -5.7±0.7 Kcal/mol
ΔS = +15±3 cal/mol*K
-TΔS = -4.4±0.8 Kcal/mol
ΔG = -10.2±0.1 Kcal/mol

Isothermal titration calorimetry (ITC) thermographs, integrated heat values and fitted parameters for titrations of BID BH3 peptide into free BCL-xLΔC or BCL-xLΔC which had been pre-incubated with an excess of the indicated p53 constructs,
p53 concentrations were sufficient to drive complex formation with BCL-xL. Binding of p53 to BCl-xL does not noticeably alter the ability of the latter protein to interact with the BID BH3 domain; however it alters the thermodynamic parameters of complex formation. The presence of p53 constructs that contain the DBD region but not the NTD slightly enhances binding of BID BH3 to BCL-xL.

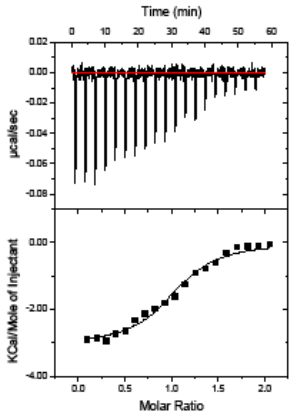

Bcl-xLΔC Wild Type
N = 1.12±0.08
K_D= 570±50 nM
ΔH = -3.04±0.04 Kcal/mol
ΔS = +18.4±0.3 cal/mol*K
-TΔS = -5.48±0.09 Kcal/mol
ΔG = -8.52±0.05 Kcal/mol

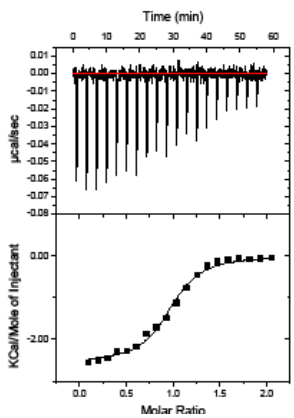

Bcl-xLΔC K20A
N = 1.1±0.1
K_D= 600±300 nM
ΔH = -2.4±0.2 Kcal/mol
ΔS = +20.7±0.5 cal/mol*K
-TΔS = -6.2±0.1 Kcal/mol
ΔG = -8.6±0.3 Kcal/mol

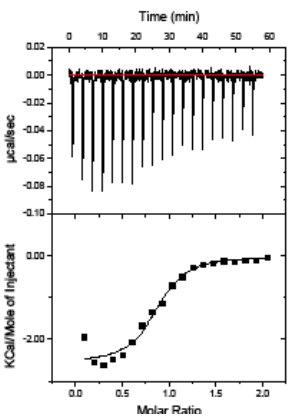

Bcl-xLΔC R103E
N = 1.0±0.1
K_D= 450±140 nM
ΔH = -2.4±0.1 Kcal/mol
ΔS = +21.0±0.3 cal/mol*K
-TΔS = -6.24±0.07 Kcal/mol
ΔG = -8.7±0.2 Kcal/mol

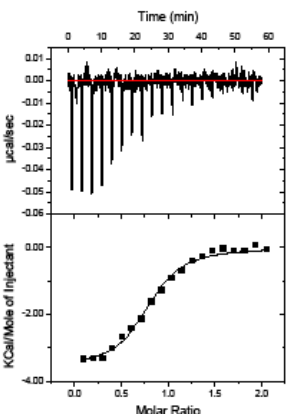

Bcl-xLΔC F105A
N = 0.74±0.05
K_D= 340±140 nM
ΔH = -3.1±0.5 Kcal/mol
ΔS = +19±2 cal/mol*K
-TΔS = -5.8±0.7 Kcal/mol
ΔG = -8.9±0.3 Kcal/mol

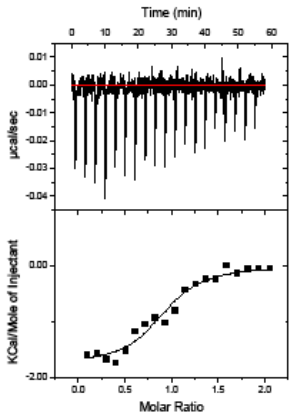

Bcl-xLΔC H113A
N = 0.96±0.04
K_D= 520±50 nM
ΔH = -1.5±0.2 Kcal/mol
ΔS = +24±1 cal/mol*K
-TΔS = -7.0±0.3 Kcal/mol
ΔG = -8.57±0.08 Kcal/mol

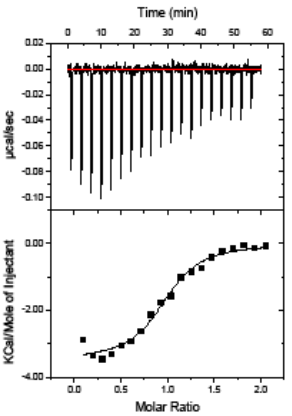

Bcl-xLΔC I114A
N = 1.03±0.06
K_D= 530±80 nM
ΔH = -3.3±0.2 Kcal/mol
ΔS = +17.8±4 cal/mol*K
-TΔS = -5.3±0.1 Kcal/mol
ΔG = -8.6±0.1 Kcal/mol

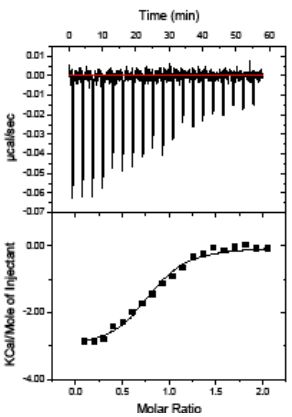

Bcl-xLΔC D156K
N = 1.0±0.2
K_D= 640±60 nM
ΔH = -2.6±0.5 Kcal/mol
ΔS = +20±2 cal/mol*K
-TΔS = -5.9±0.5 Kcal/mol
ΔG = -8.44±0.05 Kcal/mol

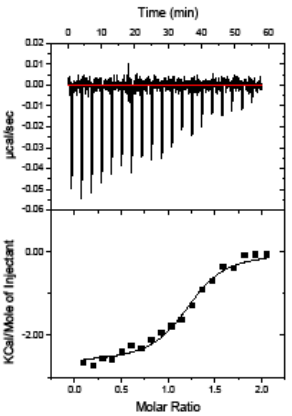

Bcl-xLΔC E158K
N = 1.0±0.2
K_D= 430±60 nM
ΔH = -2.2±0.5 Kcal/mol
ΔS = +22±1 cal/mol*K
-TΔS = -6.5±0.4 Kcal/mol
ΔG = -8.69±0.08 Kcal/mol

Isothermal titration calorimetry (ITC) thermographs, integrated heat values and fitted parameters for titrations of BAX BH3 peptide into wild-type and mutated BCL-xLΔC.

While the studied mutations impair the ability of BCL-xL to bind p53, they result in only marginal variations in its binding affinity for BH3 domains such as the BAX BH3 peptide employed in these titrations.

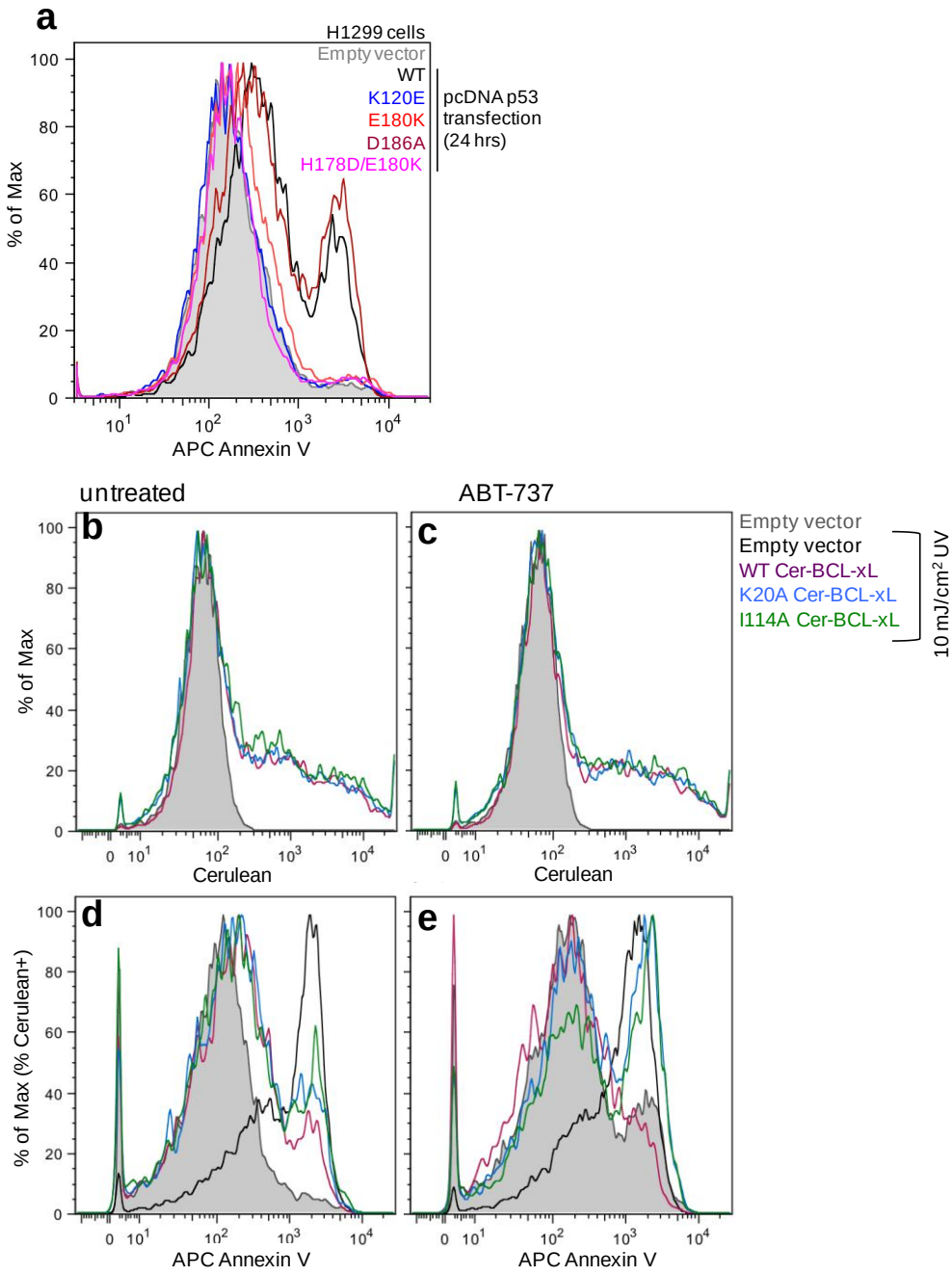

Fluorescence Activated Cell Sorting (FACS) population histograms.
a. Population distribution histograms for AnnexinV staining of H1299 cells transfected for 24 hours with p53 constructs as indicated. **b.** Population distribution histograms for Cerulean levels in cells transfected with Cerulean BCL-xL constructs as indicated. **c**. Equivalent plot for cells treated with 1 mM ABT-737 immediately after irradiation. **d.** Population distribution histograms for AnnexinV in cells transfected with empty vector in the absence or presence of 10 mJ/cm^2 UV irradiation and cells that were UV irradiated after 24 hours transfection with Cerulean BCL-xL constructs as indicated. **e**. Equivalent plot for cells treated with 1 mM ABT-737 immediately after irradiation.